Oxidation behavior of cobalt nanoparticles studied by in situ environmental transmission electron microscopy

Zhang, Dejiong; Jin, Chuanhong; Li, Z. Y.; Zhang, Ze; Li, Jixue

DOI:
10.1016/j.scib.2017.05.003

Document Version
Peer reviewed version

Citation for published version (Harvard):
Zhang, D, Jin, C, Li, ZY, Zhang, Z & Li, J 2017, 'Oxidation behavior of cobalt nanoparticles studied by in situ environmental transmission electron microscopy', *Science Bulletin*, vol. 62, no. 11, pp. 775-778. https://doi.org/10.1016/j.scib.2017.05.003

Article

Oxidation behavior of cobalt nanoparticles studied by *in situ* environment transmission electron microscopy

Dejiong Zhang, Chuanhong Jin, Z.Y. Li, Ze Zhang, Jixue Li

PII: S2095-9273(17)30243-8
DOI: http://dx.doi.org/10.1016/j.scib.2017.05.003
Reference: SCIB 130

To appear in: *Science Bulletin*

Received Date: 17 April 2017
Revised Date: 28 April 2017
Accepted Date: 2 May 2017

Please cite this article as: D. Zhang, C. Jin, Z.Y. Li, Z. Zhang, J. Li, Oxidation behavior of cobalt nanoparticles studied by *in situ* environment transmission electron microscopy, *Science Bulletin* (2017), doi: http://dx.doi.org/10.1016/j.scib.2017.05.003

Article
Received 17 April 2017
Received in revised form 28 April 2017
Accepted 2 May 2017

Oxidation behavior of cobalt nanoparticles studied by *in situ* environment transmission electron microscopy

Dejiong Zhang[a] · Chuanhong Jin[a]* · Z. Y. Li[b] · Ze Zhang[a] · Jixue Li[a]*

[a] State Key Laboratory of Silicon Materials, School of Materials Science and Engineering, Zhejiang University, Hangzhou 310027, China.

[b] Nanoscale Physics Research Laboratory, School of Physics and Astronomy, University of Birmingham, Birmingham, B152TT, UK

e-mail: chhjin@zju.edu.cn; jx_li@zju.edu.cn

Abstract The dynamics of oxidation of cobalt nanoparticles were directly revealed by in situ environmental transmission electron microscopy. Firstly, cobalt nanoparticles were oxidized to polycrystalline cobalt monoxide, then to polycrystalline tricobalt tetroxide, in the presence of oxygen with a low partial pressure. Numerous cavities (or voids) were formed during the oxidation, owing to the Kirkendall effect. Analysis of the oxides growth suggested that the oxidation of cobalt nanoparticles followed a parabolic rate law, which was consistent with diffusion-limited kinetics. In situ transmission electron microscopy allowed potential atomic oxidation pathways to be considered. The outward diffusion of cobalt atoms inside the oxide layer controlled the oxidation, and formed the hollow structure. Irradiation by the electron beam, which destroyed the sealing effect of graphite layer coated on the cobalt surface and resulted in fast oxidation rate, played an important role in activating and promoting the oxidations. These findings further our understanding on the microscopic kinetics of metal nanocrystal oxidation and knowledge of energetic electrons promoting oxidation reaction.

Keywords Cobalt · Nanoparticle · Oxidation dynamics · Parabolic rate ·Environmental transmission electron microscopy (ETEM) · Electron irradiation

1 Introduction

The oxidation of metals is a natural occurring process that affects their stability. Such oxidation can either form a protective layer at high temperatures, which may result in corrosion resistance, or alternatively cause the environmental failure [1,2]. The latter is particularly of concern when the metal size shrinks to the nanoscale, i.e., nanoparticles (NPs). Cobalt (Co) is no exception. Co NPs are usually applied in hydrogenation reactions, magnetic data storage, and biotechnology [3-6]. An oxidized form of Co NPs, Co_3O_4, has shown potential as cathode materials in lithium ion batteries, gas sensors, and

catalysis [7,8]. Co is typically oxidized into two forms of products: cobalt monoxide (CoO, Co^{2+}) and/or tricobalt tetroxide (Co_3O_4, a mixture of Co^{2+} and Co^{3+}). The product ratio depends on the oxidation conditions [2,9-17]. Understanding how these oxides are transformed during the metal oxidation, particularly from a microscopic viewpoint, could help clarify the associated mechanisms. Direct observations with techniques such as in situ transmission electron microscopy (TEM) can help address these issues.

Environmental TEM (ETEM) is useful for investigating dynamic behavior during the nanoscale structural and chemical evolution of materials under reactor conditions. It can reveal the reaction pathways of metal NPs via direct observations of intermediate phases and/or structures [18-23]. Uchiyama et al. [18] reported that the change in morphology correlated well with the catalytic activity of supported Au NPs on CeO_2. Yuan et al. [19] studied the stress-induced surface reconstruction of anatase TiO_2 in the presence of oxygen via ETEM. However, the kinetics of the oxidation of Co NPs have been less studied, particularly at the atomic scale. Herein, we report in situ observations of the thermal oxidation of Co NPs in an oxygen environment by ETEM. Microscale processes occurring during oxidation to the associated products are observed and analyzed. The growth dynamics of oxide layer are quantified, confirming that the oxidation is diffusion-limited. The effect of electron beam irradiation on the oxidation of Co NPs is also addressed.

2 Methods

Co NPs were used as received (Sigma-Aldrich, USA). They were dispersed in ethanol before being loaded onto a molybdenum TEM grid. As shown in Fig. S1 (online), sample pre-checking via a TEM (Tecnai G2 F20 S-twin, FEI, Netherland) confirmed that the Co NPs were approximately 5−50 nm in diameter, with a spherical morphology and face-centered cubic (fcc) structure. Covering of about 2-nm-thick graphite layer coated the pristine metal NPs and no oxide phase was observed. In situ experiments were performed inside an ETEM (H-9500, Hitachi, Japan) equipped with a side-entry heating and gas-injection holder. The microscope was operated at an accelerating voltage of 300 kV. The partial pressure of oxygen was stabilized at 2×10^{-2} Pa for experiments. Oxidized products were also characterized in-depth via a Cs-corrected TEM (Titan Chemi-Stem, FEI, Netherland) with super energy-dispersive X-ray spectroscopy (EDS), which was operated at an accelerating voltage of 200 kV.

3 Results and discussion

Time-sequenced TEM images in Fig. 1 show a typical oxidation process of a spherical Co NP, which has a diameter of approximately 17 nm, and a thin graphite coating layer. In the first stage, the sample was heated to 300 °C, and maintained for about 30 min under an O_2 atmosphere (2×10^{-2} Pa). The electron beam was switched off during this process, except for a very short period of sample checking procedure at the beginning. No noticeable oxidation was observed on the Co NP after the heating, as shown in Fig. 1a (image marked 0 s). The electron beam (300 kV, 1.2 A/cm^2) was then switched on for the in situ recording and observation. After approximately 32.3 s, a nanoisland (protrusion) appeared locally on the

graphite surface, as indicated by the white arrow in Fig. 1b. Its lattice fringe spacing of 0.212 nm corresponded to the (200) spacing in CoO. Therefore, the nanoisland was assigned to CoO, which is an oxidized product of Co NPs. This assignment was assisted by ex-situ high-resolution (HR) TEM characterizations, such as the partially oxidized Co NPs shown in Fig. S2 (online). As the oxidation proceeded, the CoO nanoisland grew laterally along the outermost surface of the graphite layer. Newly formed CoO nanoislands were also observed at different sites of the graphite surface, as shown in Fig. 1c. The CoO islands further developed into a continuous layer covering the entire metal surface, thus forming a core-shell structure. The metallic Co core became smaller as serving as the metal source for oxidation, until fully sacrificed. The oxide shell became increasingly thicker, as shown in Fig. 1d, e. Small cavities/voids were observed around the Co/oxide interface, as shown in Figs. 1e and S3 (online). These were a result of the Kinkendall effect, which will be discussed later. Finally, the Co NP was fully oxidized to a hollow structure, as shown in Fig. 1f. Ex-situ HRTEM images and chemical analyses shown in Fig. S2c, d (online) confirmed that the fully oxidized product layer was polycrystalline Co_3O_4, rather than CoO, evidencing that the as-formed CoO was further oxidized to Co_3O_4.

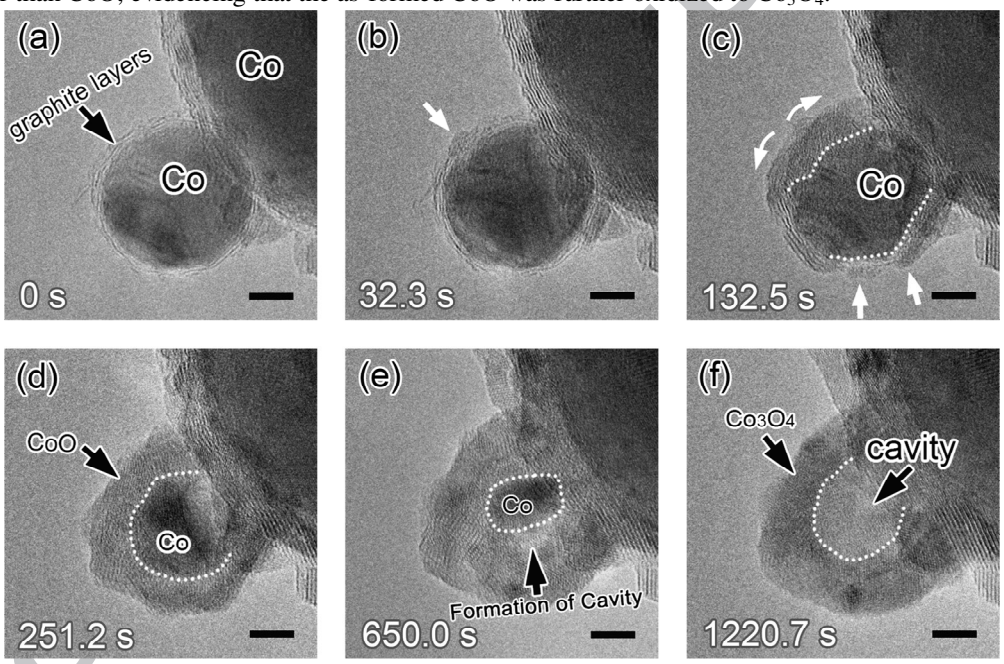

Fig. 1 Time sequential TEM images showing the oxidation of a spherical Co NP under an electron beam intensity of 1.2 A/cm^2, temperature of 300 °C, and O_2 partial pressure of 2×10^{-2} Pa. Images recorded at (a) 0, (b) 32.3, (c) 132.5, (d) 251.2, (e) 650.0, and (f) 1,220.7 s. Under electron irradiation, the surface graphite layer on the Co NP initially broke, and these breaks became the active sites for oxidation. Co was oxidized to polycrystalline CoO firstly, and further oxidized to polycrystalline Co_3O_4 with an internal cavity. Oxidation showed no crystal preference for oxides growth. Scale bars are 5 nm.

To investigate the effect of electron beam irradiation on oxidation, more experiments were carried out under different electron beam intensities, being 1.2 (sample A), 3.6 (sample B), and 9 (sample C) A/cm^2. ETEM images of the resulting process are shown in the left panel of Fig. 2. The temperature was 300 °C, and the O_2 partial pressure was 2×10^{-2} Pa, which were same as that used in Fig. 1. Oxidation of

the Co NPs (with an approximate diameter of 20 nm) again commenced only upon the electron beam irradiation. The Co NPs were similarly oxidized to form hollow structures (Fig. 2c, f, i). Comparing results from samples A and C showed that oxidation proceeded faster as the electron beam intensity was increased, while other conditions remained unchanged. Moreover, the oxidation dynamics were quantitatively analyzed based on the results of in situ TEM images. In Fig. 2j, the reaction time (y axis) is plotted as a function of the thickness of as-formed oxide layer (x axis). It was found that the data point for samples A, B, C could be well fitted by the parabolic formula, written as $t=a+cx^2$, in which x is the thickness of the oxide layer at an oxidative reaction time t ($t\geq 0$), and a, c are the fitting constants. The parabolic fitting formulas were $t=31.8+12.7x^2$, $t=37.7+11.3x^2$, $t=-1.5+6.3x^2$, for samples A, B, and C, respectively. Adj. R-square (coefficient of determination) for the corresponding three fitting outcomes were 0.9968, 0.9950 and 0.9890 (Note: there may have been some uncertainty in determining the zero point for time, but this did not affect the primary fitting results discussed here). Wagner oxidation theory [1] indicates that the parabolic oxidation behavior should have resulted from an ion-diffusion dominated reaction. For comparison, a linear rate law should be observed when reaction dominates. Accordingly, it was concluded that the oxidation of Co NPs was controlled by ion diffusion, which would further determine the microstructures of the oxidation products. After the continuous oxide layer formed, the inward transportation of oxygen ions and/or the outward diffusion of metal (Co) ions could have led to further growth of oxide layer, either at the Co/oxide interface or the oxide/O_2 interface, respectively. A significant difference in ion diffusion coefficients (so called Kirkendall effect), and accumulation of vacancies at the metal/oxide interface, would have led to the formation of cavities [22, 24-28]. In Figs. 1 and S3 (online), the formation of cavities at the Co/oxides interface and hollow oxide structure were observed, suggesting that the outward diffusion of Co dominated the reactions, and that oxidation occurred mainly at the oxide/O_2 interface, rather than at the Co/oxide interface. To clearly show the movement of cavity, we have colored the corresponding TEM images, as shown in Fig. S4 (online). Grain boundaries and point defects such as cobalt and oxygen vacancies occurring in the polycrystalline structures of the cobalt oxides (either CoO or Co_3O_4) would have provided pathways for the diffusion of Co [10].

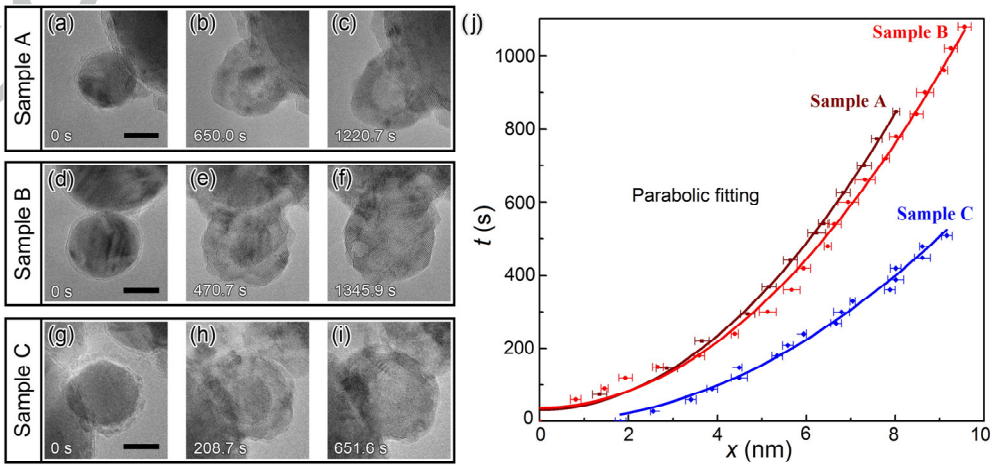

Fig. 2 (Color online) Time sequential TEM images showing the oxidation of Co NPs with similar diameters (approximately 20 nm) under different electron beam intensities of sample A, 1.2 A/cm^2 (a)−(c); sample B, 3.6 A/cm^2 (d)−(f); and sample C, 9.0 A/cm^2 (g)−(i). A temperature of 300 °C and O_2 partial pressure of 2×10^{-2} Pa were used. The surface nanoislands in Fig. 2g resulted from electron beam irradiation-induced oxidation, and occurred during the imaging alignment process. All particles were oxidized to hollow structures. Scale bars are 10 nm. (j) Quantitative analysis of the oxidation dynamics of samples A, B, and C. The thickness of the oxide layer (x) at reaction time (t) was measured with a spherical approximation, and showed parabolic fitting behavior.

The parabolic equation for oxidation can be expressed as $x^2=2k_pt$, in which x is the oxide layer thickness at time t, and k_p is the oxidation rate constant [29]. The rearranged form of this equation, $k_p=1/(2c)$, was used to calculate the oxidation (parabolic) rate constants from the above results. Values of k_p were determined to be 0.0394 nm^2/s for sample A (beam intensity of 1.2 A/cm^2), 0.0442 nm^2/s for sample B (beam intensity of 3.6 A/cm^2), and 0.0794 nm^2/s for sample C (beam intensity of 9 A/cm^2). The plotted graph for oxidation rate constant to electron beam intensity is shown in Fig. 3. It is clear that a higher electron beam intensity resulted in a higher oxidation rate constant, giving Co NPs were oxidized more rapidly when irradiated by a higher-intensity electron beam. Experiments were also carried out to investigate the influence of particle size on the oxidation of Co NPs. The results are shown in Figs. S5 and S6 (online). We demonstrated that the oxidation of Co NPs with different diameters all followed parabolic rate laws, while there was a tendency that smaller sized Co NPs had higher oxidation rate constants. This may have been due to the cause that smaller sized NPs possessed higher surface energy, so they would have performed more active upon oxidation.

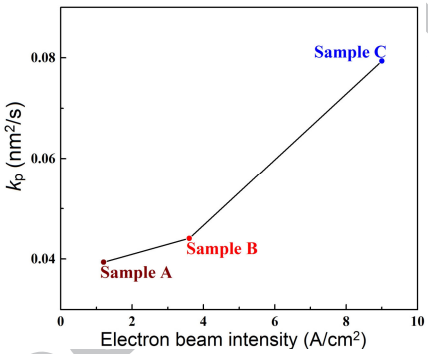

Fig. 3 (Color online) Plotted graph of calculated oxidation rate constants (k_p) to electron beam intensities. Higher the electron beam intensity, higher the oxidation rate constant.

The above oxidations were all carried out under both thermal heating (at 300 °C) and electron beam excitation. When we conducted the experiments at room temperature while setting the electron intensity at 1.2 A/cm^2 and O_2 partial pressure at 2×10^{-2} Pa (the same as previous cases), the formation of cobalt oxides with a core-shell structure and hollow structure (cavity) were also observed, as shown in Fig.4 with the time sequential TEM images. It evidenced that electron beam irradiation could trigger the oxidation of Co NPs in the absence of thermal activation. Estimates of the oxidation dynamics confirmed that the electron beam-induced oxidation followed the parabolic behavior. As shown in Fig. 4e, the

fitting formulas on measured oxide layer increasing for particles C and F were t=418.3+53.5x^2 (Adj. R-square: 0.9718) and t=405.2+60.9x^2 (Adj. R-square: 0.9376), and the k_p were 0.0094 and 0.0082 nm^2/s, respectively. Comparing with 0.0394 nm^2/s for sample A in Fig. 2, which was oxidized under both thermal heating (300 °C) and electron irradiation (1.2 A/cm^2), it was concluded that without thermal heating, the oxidation proceeded with a much slower reaction rate. We think that the thermal heating significantly promoted the diffusion of atoms (i.e., Co), which thus significantly increased the oxidation rate.

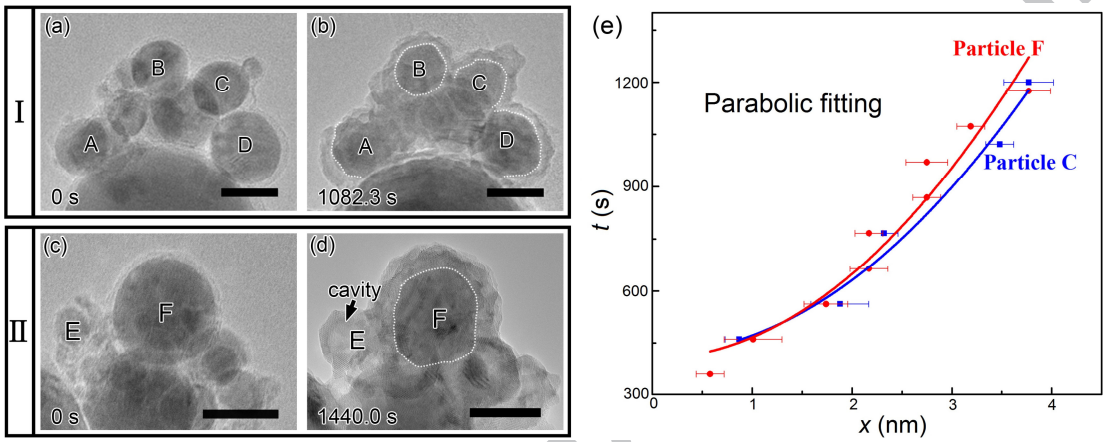

Fig. 4 (Color online) TEM images showing the oxidation of Co NPs at the room temperature induced by electron beam irradiation. The electron beam intensity was 1.2 A/cm^2, and the oxygen partial pressure was 2×10^{-2} Pa. I: (a) 0, and (b) 1,082.3 s; II: (c) 0, and (d) 1,440.0 s. The two examples were formed at the same conditions and similar times. Scale bars are 20 nm. (e) Oxidation dynamic analysis of the evolution of particles C and F. The measured variation of oxide layer thickness (x) at oxidative reaction time (t) was parabolic fitted.

The effect of energetic electron beam irradiation on the oxidations could be attributed to several possible contributions, as following: (1) It may have destroyed the sealing effect of graphite layer by creating local vacancy defects through the knock-on process [30,31], thus providing channels for the migration and diffusion of Co and oxygen. As such, outward migrated Co atoms would then have been exposed to oxygen and thus been oxidized, as shown in Fig. 1. It was also an evidence that the graphite layer functioned as a good sealing layer to prevent the penetration of metal atoms [32]. (2) The electron beam may have enhanced the diffusion of Co also through the knock-on effect [30], thus promoting oxidation. (3) Electron beam irradiation may have assisted the decomposition of O_2 into atomic oxygen, and thus enhanced oxidation [23,33,34]. The high-energy electrons directly induced the ionization and disassociation of molecular oxygen in the microscope column and on the NP surfaces. This may have activated the oxidation of the on-surface graphite layer, then the Co NP.

4 Conclusions

To summary, the parabolic oxidation behavior of Co NPs under electron beam irradiation was studied using in situ ETEM. The microstructure evolution and oxidation dynamics were investigated. Firstly, the oxidation of Co NPs formed CoO, then transformed to Co_3O_4. The outward diffusion of Co controlled the reactions, and induced vacancies within the oxide product. In addition to their role in imaging, the energetic electrons activated the oxidation directly. Higher electron beam intensities resulted in higher oxidation rates. These findings on the oxidation of Co NPs enhance our understanding on metal oxidation, and may further the use of Co NPs in their respective applications.

Acknowledgments This work was supported by the National Natural Science Foundation of China (11227403, 51472215, 51222202), the National Basic Research Program of China (2014CB932500, 2015CB921004) and Cyrus Tang Center for Sensor Materials and Applications. This work made use of the resources of the Center of Electron Microscopy of Zhejiang University (ZJU). Z.Y. Li thanks the Qiushi Foundation for the visiting professorship in ZJU.

Conflict of Interest The authors declare that they have no conflict of interest.

References

1. Atkinson A (1985) Transport processes during the growth of oxide-films at elevated-temperature. Rev Mod Phys 57: 437-470
2. Martin M, Koops U, Lakshmi N (2004) Reactivity of solids studied by in situ XAS and XRD. Solid State Ionics 172: 357-363
3. Silva DO, Scholten JD, Gelesky MA, et al (2008) Catalytic gas-to-liquid processing using cobalt nanoparticles dispersed in imidazolium ionic liquids. ChemSusChem 1: 291-294
4. Khadzhiev SN, Krylova AY (2011) Fischer-tropsch synthesis in a three-phase system over nanocatalysts (review). Petrol Chem 51: 74-85
5. Lu AH, Li WC, Matoussevitch N, et al (2004) Highly stable carbon-protected cobalt nanoparticles and graphite shells. Chem Commun, 1: 98-100
6. Pedro T, María del Puerto M, Sabino VV, et al (2003) The preparation of magnetic nanoparticles for applications in biomedicine. J Phys D Appl Phys 36: R182
7. Li WY, Xu LN, Chen J (2005) Co_3O_4 nanomaterials in lithium-ion batteries and gas sensors. Adv Funct Mater15: 851-857
8. Deng XH, Tüysüz H (2014) Cobalt-oxide-based materials as water oxidation catalyst: recent progress and challenges. ACS Catal 4: 3701-3714
9. Chernavskii PA, Pankina GV, Zaikovskii VI, et al (2008) Formation of hollow spheres upon oxidation of supported cobalt nanoparticles. J Phys Chem C 112: 9573-9578
10. Ha DH, Moreau LM, Honrao S, et al (2013) The oxidation of cobalt nanoparticles into kirkendall-hollowed CoO and Co_3O_4: the diffusion mechanisms and atomic structural transformations. J Phys Chem C 117: 14303-14312

11. Saric I, Peter R, Petravic M (2016) Oxidation of cobalt by oxygen bombardment at room temperature. J Phys Chem C 120: 22421-22425
12. Cazacu A, Larosa C, Beaunier P, et al (2014) Self-organization and/or nanocrystallinity of Co nanocrystals effects on the oxidation process using high-energy electron beam. Adv Funct Mater 24: 164-170
13. Xin HL, Niu K, Alsem DH, et al (2013) In situ TEM study of catalytic nanoparticle reactions in atmospheric pressure gas environment. Microsc Microanal 19: 1558-1568
14. Mrowec S, Przybylski K (1977) Oxidation of cobalt at high temperature. Oxid Met 11: 365-381
15. Gulbransen EA, Andrew KF (1951) The kinetics of the oxidation of cobalt. J Electrochem Soc 98: 241-251
16. Sheasby JS, Gleeson B (1989) Oxygen tracer study of the high-temperature oxidation of pure and impure cobalt. Oxid Met 32: 379-390
17. Tompkins HG, Augis JA (1981) The oxidation of cobalt in air from room-temperature to 467 °C. Oxid Met 16: 355-369
18. Uchiyama T, Yoshida H, Kuwauchi Y, et al (2011) Systematic morphology changes of gold nanoparticles supported on CeO_2 during Co oxidation. Angew Chem Int Ed 50: 10157-10160
19. Yuan W, Wang Y, Li H, et al (2016) Real-time observation of reconstruction dynamics on TiO_2(001) surface under oxygen via an environmental transmission electron microscope. Nano Lett 16: 132-137
20. Ward MR, Boyes ED, Gai PL (2013) In situ aberration-corrected environmental TEM: reduction of model Co_3O_4 in H_2 at the atomic level. ChemCatChem 5: 2655-2661
21. Jeangros Q, Hansen TW, Wagner JB, et al (2014) Oxidation mechanism of nickel particles studied in an environmental transmission electron microscope. Acta Mater 67: 362-372
22. Wang CM, Genc A, Cheng H, et al (2014) In-situ TEM visualization of vacancy injection and chemical partition during oxidation of Ni-Cr nanoparticles. Sci Rep 4: 3683
23. Yoshida H, Omote H, Takeda S (2014) Oxidation and reduction processes of platinum nanoparticles observed at the atomic scale by environmental transmission electron microscopy. Nanoscale 6: 13113-13118
24. Yin Y, Rioux RM, Erdonmez CK, et al (2004) Formation of hollow nanocrystals through the nanoscale Kirkendall effect. Science 304: 711-714
25. Fan HJ, Knez M, Scholz R, et al (2007) Influence of surface diffusion on the formation of hollow nanostructures induced by the kirkendall effect: the basic concept. Nano Lett 7: 993-997
26. Pratt A, Lari L, Hovorka O, et al (2014) Enhanced oxidation of nanoparticles through strain-mediated ionic transport. Nat Mater 13: 26-30
27. Wang X, Feng J, Bai Y, et al (2016) Synthesis, properties, and applications of hollow micro-/nanostructures. Chem Rev 116: 10983-11060
28. Zhang B, Fan H, Bian T, et al (2013) Synthesis of mesoporous hollow inorganic micro-/nano-structures via self-templating methods. Chem J Chin Univ 34: 1-14
29. Cabrera N, Mott NF (1949) Theory of the oxidation of metals. Rep Prog Phys 12: 163-184

30. Egerton RF, Li P, Malac M (2004) Radiation damage in the TEM and SEM. Micron 35: 399-409
31. Banhart F, Li JX, Krasheninnikov AV (2005) Carbon nanotubes under electron irradiation: stability of the tubes and their action as pipes for atom transport. Phys Rev B 71: 241408
32. Banhart F, Grobert N, Terrones M, et al (2001) Metal atoms in carbon nanotubes and related nanoparticles. Int J Mod Phys B 15: 4037-4069
33. Huang X, Jones T, Fan H, et al (2016) Atomic-scale observation of irradiation-induced surface oxidation by in situ transmission electron microscopy. Adv Mater Interfaces 3: 1600751
34. Zhang D, Jin C, Tian H, et al (2017) An in situ TEM study of the surface oxidation of palladium nanocrystals assisted by electron irradiation. Nanoscale DOI: 10.1039/C6NR08763A